

## Chaotification of Sine-series maps based on the internal perturbation model

Chunyi Dong <sup>a</sup>, Karthikeyan Rajagopal <sup>b</sup>, Shaobo He <sup>a,\*</sup>, Sajad Jafari <sup>c</sup>, Kehui Sun <sup>a</sup>

<sup>a</sup> School of Physics and Electronics, Central South University, Changsha 410083, China

<sup>b</sup> Center for Nonlinear Systems, Chennai Institute of Technology, Chennai, India

<sup>c</sup> Health Technology Research Institute, Amirkabir University of Technology, No. 350, Hafez Ave, Valiasr Square, Tehran 159163-4311, Iran

### ARTICLE INFO

**Keywords:**  
Chaos  
Chaotification  
Perturbation  
Discrete map  
Complexity

### ABSTRACT

In this paper, a chaotification method based on the internal perturbation model (IPM) is proposed. The single-perturbation and the multiple-perturbations are introduced. The Sine map is taken as an example. Moreover, this method can be generalized to high-dimensional maps that contain sine, no matter where the sine term is in the system equation. we further apply IPM to an integer-order and a fractional-order Sine-series map. For those new maps, the parameter space and FuzzyEn complexity are significantly extended while maintaining the topological structure of system. These complex behaviors and digital signal processing (DSP) implementation validate the effectiveness of IPM and make it have the potential of better secure communication and encryption.

### Introduction

In 1963, Lorenz discovered that a small deviation in the initial conditions could lead to huge differences in the calculations of the meteorological system [1]. Later, Robert reported the Logistic map [2] in 1976 and it opened a precedent for the study of discrete chaotic systems. Recent studies show that discrete systems widely exist in many research fields, including image encryption [3], system control [4], neuron network [5], viscoelastic materials [6], random signal generator [7], biological mechanism [8] and so on [9,10].

However, the existing chaotic systems have some limitations which are presented as follows: (1) The parameters and dynamic behaviors of many chaotic systems can be predicted by the initial state and trajectory [11,12]. (2) Slight changes of parameters may destroy the chaotic characteristics of systems [13]. (3) The finite precision effect will cause the chaotic degradation of the system with weak ergodicity [14]. (4) The initial value sensitivity of the chaotic system may lead to the coexistence of periodic and chaotic states [15]. These phenomena limit the application of chaotic system. Therefore, if the discrete chaotic system has better ergodicity and larger chaotic range, it will be more resistant to the above limitations.

In order to overcome the aforementioned problems, the enhanced chaotic maps are proposed in various ways, such as memristor [16], physical models [17,18], dimension expansion [19,20], cascaded chaos [21], offset boosting [22] and fractional-order expansion [23,24]. Bao et al. proposed a general DM model based on the nonlinearity of memristor [25], coupled the discrete memristor with 2D discrete maps, and generated four cases of 3D-DM maps with no or infinitely many

fixed points [26]. In addition, the participation of memristor can better simulate the magnetic induction effect of biological neurons [27]. Li et al. [28] extended the 1D Chebyshev to 2D Chebyshev, and Hua et al. [29] concatenated two 1D chaotic maps. Wu et al. [30] expanded the classic 1D Logistic map to a 2D Logistic map by establishing a closed-loop coupling mechanism, which can improve the complexity of the systems. Yuan et al. [31] proposed a method to construct the new discrete chaotic system through self-cascading and mutual cascading. Hua et al. [12] introduced a sine chaotification model (SCM) as a general framework to enhance the chaos complexity of existing chaotic maps. Although it is a simple method, each dimension of the system is used as the input of the Sine map, resulting in the output range being limited to  $[-1, 1]$ , and the ergodicity of the system will be affected. Li et al. [32] proposed the fractional difference form of sine chaotification model (FSCM) to improve the chaos complexity of existing chaotic maps. This method expands the range of SCM output, but the application of fractional-order also brings higher implementation costs.

Though these proposed methods can improve the performance of the system, they may cause high cost and complex mathematical structure when applied to the high-dimensional systems. Thus, based on the initial value sensitivity of chaotic system, this paper proposes a chaotification method by the internal perturbation model (IPM). Moreover, Sine map [33] is involved in the construction and modulation of many high-dimensional chaotic systems. We consider whether we can further improve the performance of the systems that contain Sine by the chaotification of Sine map, no matter where the Sine term is in the system equation. It is worth mentioning that for high-dimensional

\* Corresponding author.

E-mail address: [heshabo@csu.edu.cn](mailto:heshabo@csu.edu.cn) (S. He).

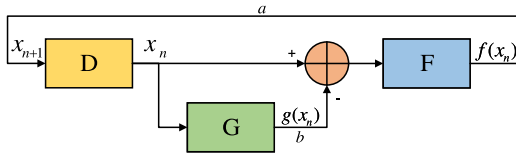


Fig. 1. Block diagram of the internal perturbation model.

**Table 1**  
Categories of single-perturbation.

$g(x)$	Non/linear	Non/periodic	Un/bounded
$x$	Linear	Non-periodic	Unbounded
$e^x$	Non-linear	Non-periodic	Unbounded
$\cos x$	Non-linear	Periodic	Bounded
$\cos(\frac{x}{x})$	Non-linear	Non-periodic	Bounded

map with Sine term, the introduction of IPM will not only maintain its topological structure, but also make its distribution more uniform.

The rest of this paper is presented as follows. In Section “Internal perturbation model”, the definition of the perturbation controller IPM and the choices of perturbation functions are given. Section “Case with single-perturbation” applies IPM with single-perturbation to Sine map. In Section “Case with multiple-perturbations”, we apply IPM with multiple-perturbations to three maps and analyze the dynamics of the enhanced maps and introduce DSP for verification. Finally, the conclusions are summarized and the future research directions are pointed out.

## Internal perturbation model

### Presentation of IPM

The proposed internal perturbation model IPM is designed to enhance the chaos complexity of existing maps. Take chaotic map  $f(x)$  as the basic map and use  $g(x)$  to perturb it. Then, IPM is defined as:

$$x_{n+1} = f(x_n - bg(x_n)). \quad (1)$$

Among this, the input of  $f(x)$  is regulated by the perturbation function  $g(x)$  and  $b$  is the control parameter of  $g(x)$ . The generated perturbation can add one more loop in each iteration.

According to the number of perturbation functions, IPM has two forms:

#### single-perturbation and multiple-perturbations.

The effective perturbation is screened out through IPM with single-perturbation, and then  $g(x)$  is superimposed on the system through IPM with multiple-perturbations.

The block diagram of IPM with single-perturbation is illustrated in Fig. 1. Here  $D$  is a unit delay.  $F$  generates the basic system  $f(x)$ , and  $G$  provides perturbation terms  $g(x)$  to regulate the system. The details of  $g(x)$  are shown in Table 1. In real applications, the choice of  $g(x)$  is determined by numerical analysis.

As shown in Eq. (2), for IPM with multiple-perturbations,  $g(x)$  is the superposition of multiple single-perturbations and the block diagram is shown in Fig. 2. Here  $G_i$  provides different perturbations  $g_i(x)$  to modulate the system.

$$g(x) = g_1(x) + g_2(x) + \dots \quad (2)$$

### Proof of existence of chaos

#### (1) Equilibrium point analysis

The equilibrium point equation of Eq. (1) with single/multiple-perturbation is expressed as

$$x = f(x - bg(x)). \quad (3)$$

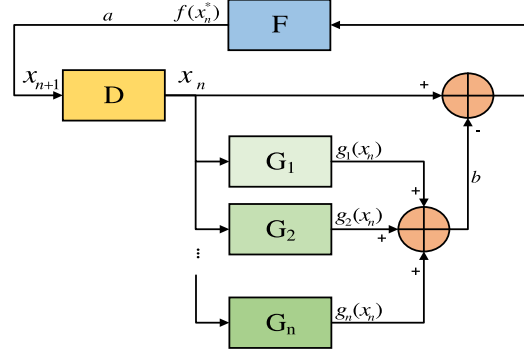


Fig. 2. Block diagram of IPM with multiple-perturbations.

Let  $y_1 = x$ ,  $y_2 = f(x - bg(x))$ , the existence of the equilibrium point is equivalent to the existence of the intersection of  $y_1$  and  $y_2$ . The specific analysis of the equilibrium point will be pointed out in Subsection “The enhanced Sine map”.

#### (2) Lyapunov exponents

**Theorem 1.** For  $f(x) \in D$ ,  $g(x) \in D$ ,  $x \in D$  on the same domain, where  $D$  is the bounded domain. If  $f(x)$  is chaotic, the IPM of  $f(x)$  is chaotic.

**Proof.** The Lyapunov exponent of a chaotic map  $f(x)$  is defined as

$$LE_f = \lim_{n \rightarrow \infty} \frac{1}{n} \sum_{i=0}^{n-1} \ln |f'(x_i)| = f > 0, \quad x_i \in D. \quad (4)$$

Since  $f(x) \in D$ ,  $g(x) \in D$ ,  $x \in D$ , it can be verified as  $f(x - bg(x)) \in D$ . According to Eq. (4), the Lyapunov exponent of the IPM can be further verified as

$$LE_{f\text{IPM}} = \lim_{n \rightarrow \infty} \frac{1}{n} \sum_{i=0}^{n-1} \ln |f'(x_i - bg(x_i))| > 0 \quad (5)$$

**Theorem 2.** When  $g(x)$  is increase with  $b < 0$  or decrease with  $b > 0$ ,  $LE_{f\text{IPM}} > LE_f$  is obtained.

#### Proof.

$$\begin{aligned} LE_{f\text{IPM}} &= \lim_{n \rightarrow \infty} \frac{1}{n} \sum_{i=0}^{n-1} \ln |f'(x_i - bg(x_i))(1 - bg'(x_i))| \\ &= \lim_{n \rightarrow \infty} \frac{1}{n} \sum_{i=0}^{n-1} (\ln |f'(x_i - bg(x_i))| + \ln |1 - bg'(x_i)|) \\ &= f + \lim_{n \rightarrow \infty} \frac{1}{n} \sum_{i=0}^{n-1} \ln |1 - bg'(x_i)| \end{aligned} \quad (6)$$

If  $bg'(x) < 0$ , then  $1 - bg'(x) > 0$  and  $\ln |1 - bg'(x_i)| > 0$ ,  $LE_{f\text{IPM}} > LE_f$  is obtained. There are two cases that the above conditions are met.

- (a)  $b > 0$  and  $g'(x) < 0$  ( $g(x)$  is increase).
- (b)  $b < 0$  and  $g'(x) > 0$  ( $g(x)$  is decrease).

**Theorem 3.** When  $g(x)$  is increase with  $b > 0$  or decrease with  $b < 0$ ,  $LE_{f\text{IPM}} > LE_f$  and  $LE_{f\text{IPM}}$  increases with the increase of  $|b|$ .

**Proof.** For another condition of Eq. (6), if  $bg'(x) > 2$ , then  $LE_{f\text{IPM}} > LE_f$  is obtained. There are two cases need to be discussed.

- (a) In the case of  $b > 0$  and  $g'(x) > 0$ , to meet the condition  $bg'(x) > 2$ , it can be deduced that  $g'(x) > \frac{2}{b}$ . The larger of  $b$ , the larger the value of  $\lim_{n \rightarrow \infty} \frac{1}{n} \sum_{i=0}^{n-1} \ln |1 - bg'(x_i)|$ .
- (b) In the case of  $b < 0$  and  $g'(x) < 0$ , to meet the condition  $bg'(x) > 2$ , it can be deduced that  $g'(x) < \frac{2}{b}$ . The smaller of  $b$ , the larger the value of  $LE_{f\text{IPM}}$ .

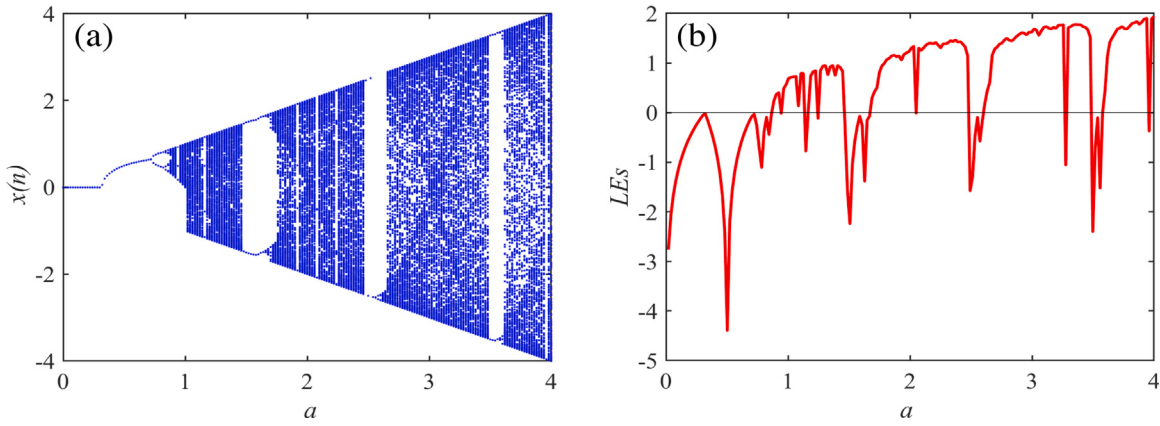


Fig. 3. (a) The bifurcation diagram of Sine map. (b) The LEs of Sine map.

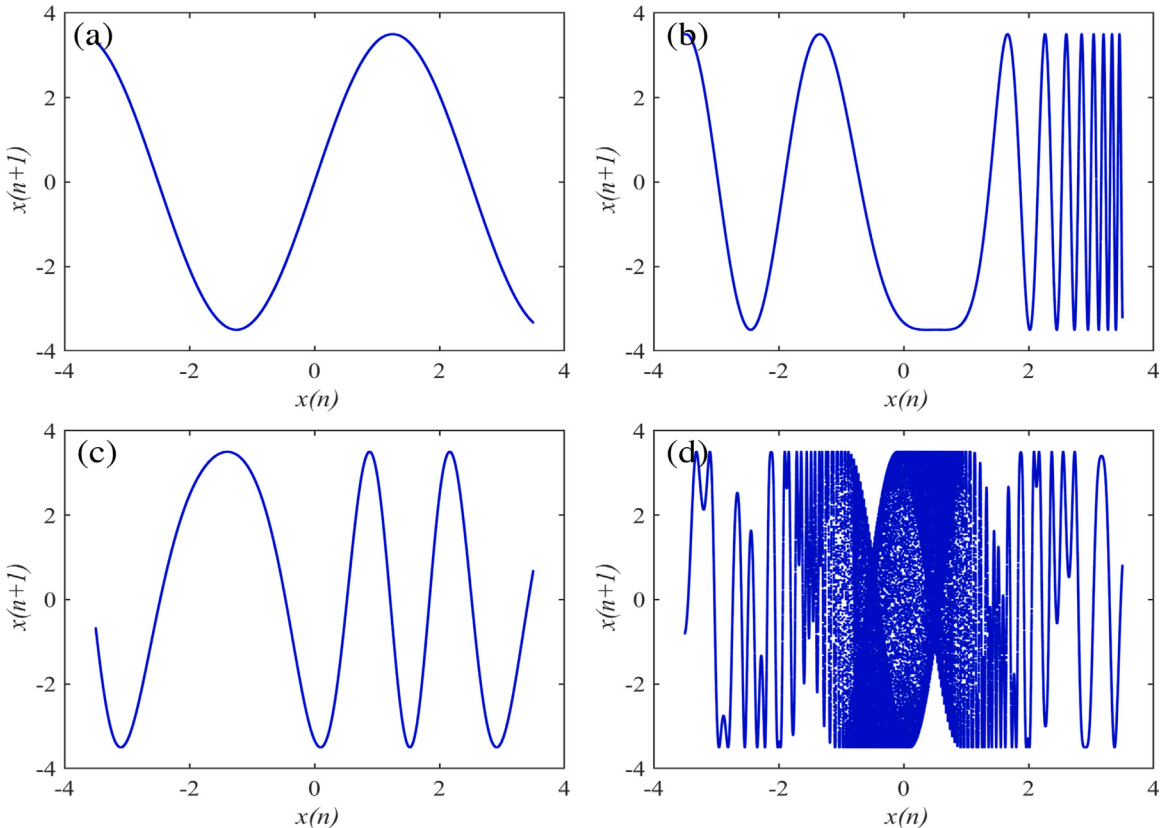


Fig. 4. The phase diagrams of IPM with different perturbations (a) IPM<sub>a</sub> (b) IPM<sub>b</sub> (c) IPM<sub>c</sub> (d) IPM<sub>d</sub>.

### Case with single-perturbation

Take Sine map as an example. In this section, IPM with single-perturbation is applied to Sine map. The dynamic characteristics of Sine map with different  $g(x)$  are analyzed to show the effectiveness of the perturbation controller.

#### Dynamics of Sine map

Firstly, it is important to clarify the extent to what Sine map needs to be improved. The Sine map is defined as:

$$x_{n+1} = a \sin(\pi x_n), \quad (7)$$

where  $a > 0$ . Let initial condition  $x_0=0.1$ ,  $a$  varies from 0 to 4 with step size 0.02. The bifurcation and Lyapunov exponents of the system

are plotted in Fig. 3. It shows that periodic windows and chaotic intervals appear with the variation of parameter  $a$ . Specifically, the period windows of Sine map are located at

$$\{a|(0 < a < 0.88) \cup (a = n + 0.5 \pm \delta, n \in N)\}.$$

#### Dynamics of Sine map with single-perturbation

The IPM with single-perturbation is applied to Sine map. In order to find the effective perturbation controller, the dynamic characteristics of IPM<sub>a-d</sub> in Table 2 are analyzed.

##### (1) Phase diagrams

Here, we set  $x_0=0.1$ ,  $a=3.5$  and  $b=0.6$ . Fig. 4 illustrates the phase diagrams of IPM<sub>a-d</sub>. It indicates different kinds of  $g(x)$  have different effects on the shape of phase diagrams. Among them, the phase diagrams of IPM<sub>a</sub> stretches the attractor of Sine map. IPM<sub>b</sub> is stretched in the

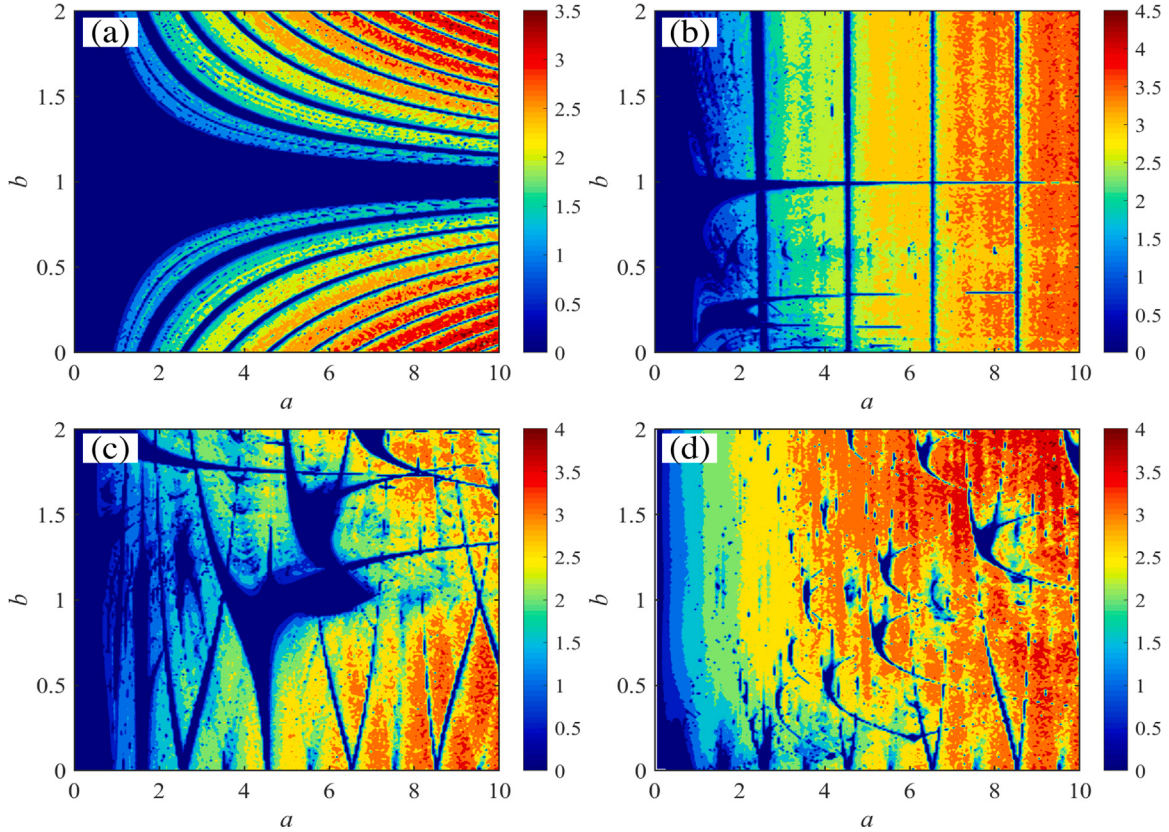


**Fig. 5.** The FuzzyEn complexity chaotic diagram of IPM with different perturbations (a)  $\text{IPM}_a$  (b)  $\text{IPM}_b$  (c)  $\text{IPM}_c$  (d)  $\text{IPM}_d$ .

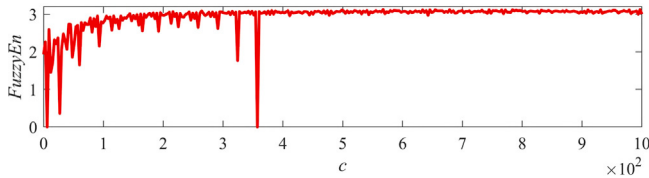


**Fig. 6.** The FuzzyEn complexity of  $\text{IPM}_d$  with variable  $c$ .

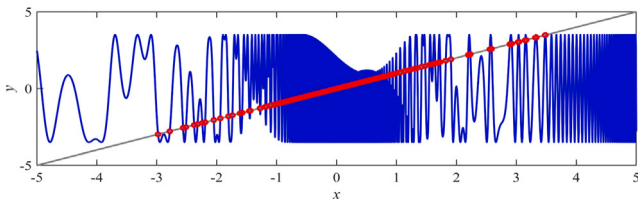


**Fig. 7.** The equilibrium points of S-IPM.

**Table 2**  
Categories of perturbation functions.

$g(x)$	Maps	Case
$x$	$x_{n+1} = a \sin(\pi(x_n - bx_n))$	$\text{IPM}_a$
$e^x$	$x_{n+1} = a \sin(\pi(x_n - be^{x_n}))$	$\text{IPM}_b$
$\cos x$	$x_{n+1} = a \sin(\pi(x_n - b \cos(x_n)))$	$\text{IPM}_c$
$\cos(\frac{x}{x_0})$	$x_{n+1} = a \sin(\pi(x_n - b \cos(\frac{x}{x_0})))$	$\text{IPM}_d$

negative interval of  $x(n)$  and compressed in the positive interval. The phase diagrams of  $\text{IPM}_c$  is unevenly distributed. When  $\cos(\frac{x}{x_0})$  is used as internal perturbation terms, the phase diagram oscillates violently

around zero and generates dense phase points. The simulation results demonstrate that IPM changes the density laterally of phase diagrams.

#### (2) FuzzyEn complexity analysis

The magnitude of the complexity measure is proportional to the randomness of the time series of the chaotic systems. Compared with ApEn [34] and SampEn algorithms, FuzzyEn algorithm is more effective. In this paper, FuzzyEn complexity algorithm is used to intuitively evaluate the randomness of the proposed chaotic maps. For the given sequence  $\{u(1), u(2), \dots, u(N)\}$ , the definition of FuzzyEn [35,36] is

$$\left\{ \begin{array}{l} \text{FuzzyEn}(m, r, N) = \ln \Phi^m(r) - \ln \Phi^{m+1}(r) \\ \Phi^m(r) = (N-m+1)^{-1} \sum_{i=1}^{N-m+1} C_i^m(r) \\ C_i^m(r) = (N-m)^{-1} \sum_{j=1, j \neq i}^{N-m+1} A_{i,j}^m \\ A_{i,j}^m = \exp(-\ln 2 \cdot (d_{i,j}^m/r)^2) \\ d_{i,j}^m = d[U^m[i], U^m[j]] = \max_{p=1,2,\dots,m} (|u(i+p+1) - u_0(i)| \\ \quad - |u(i+p+1) - u_0(j)|) \end{array} \right. \quad (8)$$

where  $m$  is the phase space dimension,  $r$  is the similarity tolerance,  $N$  is the sequence length,  $m(m \leq N-2)$  is the non-negative integer, and  $u_0(i) = \frac{1}{m} \sum_{j=0}^{m-1} u(i+j)$ . The parameters are set as  $m = 2$ ,  $r = 0.15$  and  $x_0 = 0.1$ . FuzzyEn complexity of maps with  $a$  and  $b$  are analyzed, and the results are shown in Fig. 5. The blue region has lower complexity, and it indicates the system is more predictable under the corresponding parameters. Different color corresponds different complexity. The red region indicates high complexity, complex data patterns and irregular behaviors.

As shown in Fig. 5 that the Sine map with different perturbations presents different complexity regions. Specifically, Fig. 5(a) and (c) have much wider low complexity regions in the parameter plane ( $a-b$ ). Among them, SIP<sub>b</sub> has the highest complexity value that can reach to 4.5 and the area of the low complexity region is less than other

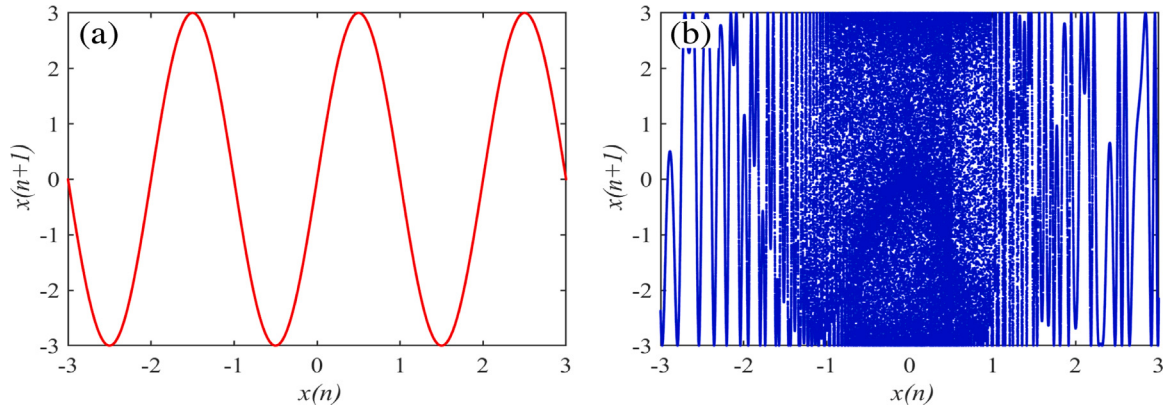
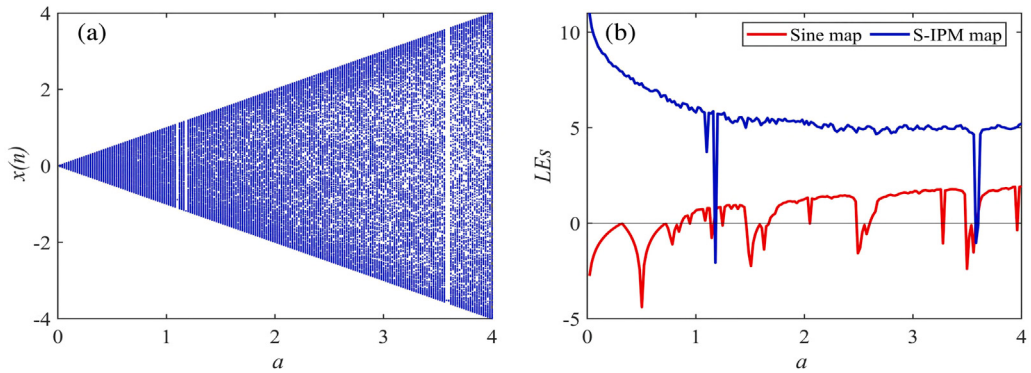
Fig. 8. The phase diagrams with  $a=3$ . (a) Sine map. (b) S-IPM with  $b=1$ .

Fig. 9. (a) The bifurcation diagram of S-IPM. (b) The Lyapunov exponents of Sine and S-IPM.

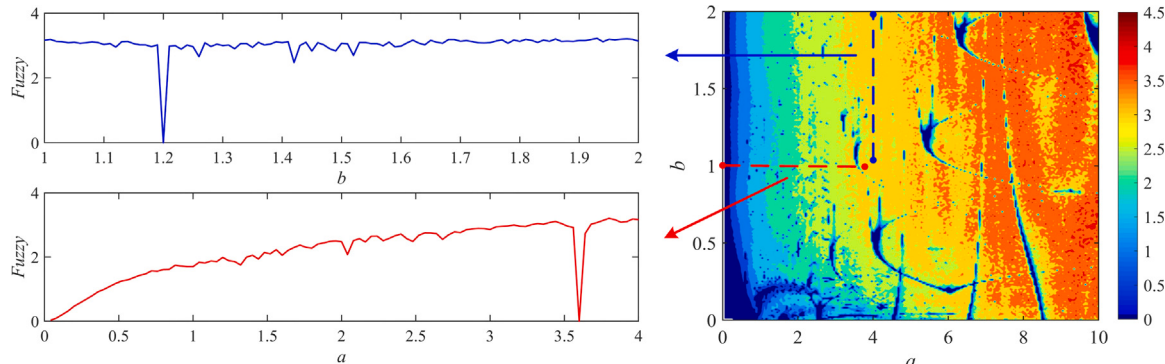


Fig. 10. FuzzyEn complexity chaos diagram of S-IPM.

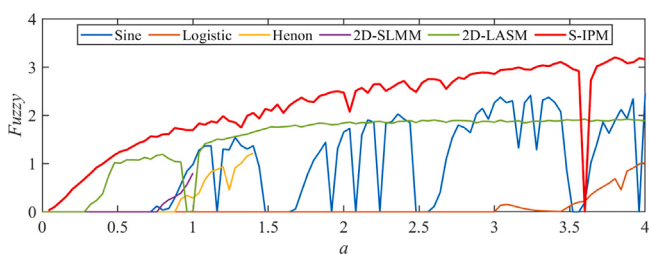
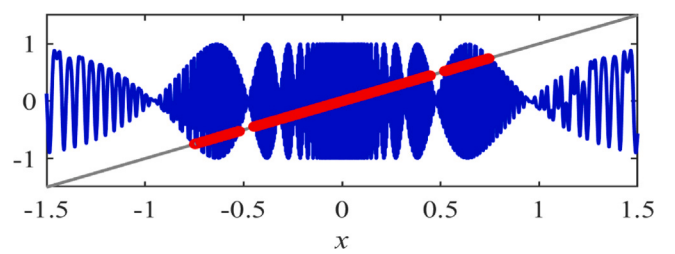
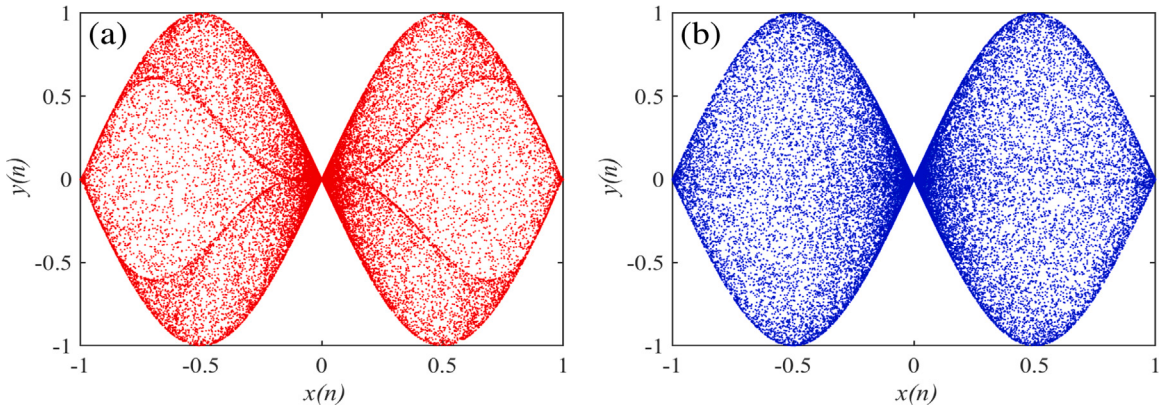
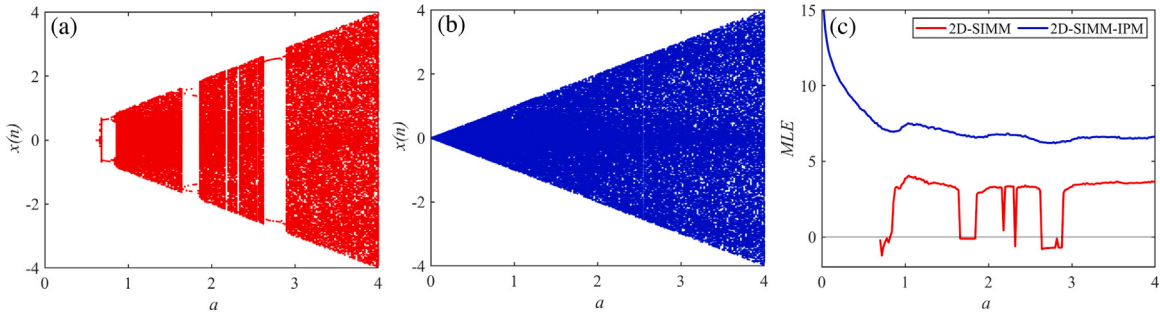
Fig. 11. FuzzyEn complexity comparison of different maps with  $a \in [0, 4]$ .

Fig. 12. The equilibrium points of 2D-SIMM-IPM.



**Fig. 13.** The phase diagrams with  $(a, \omega, \gamma) = (1, \pi, 3)$ . (a) 2D-SIMM. (b) 2D-SIMM-IPM with  $b=1$ .



**Fig. 14.** With the parameters  $(a, \omega, \gamma) = (1, \pi, 3)$ . (a) Bifurcation diagram of 2D-SIMM. (b) Bifurcation diagram of 2D-SIMM-IPM with  $b=1$ . (c) MLE of 2D-SIMM and 2D-SIMM-IPM.

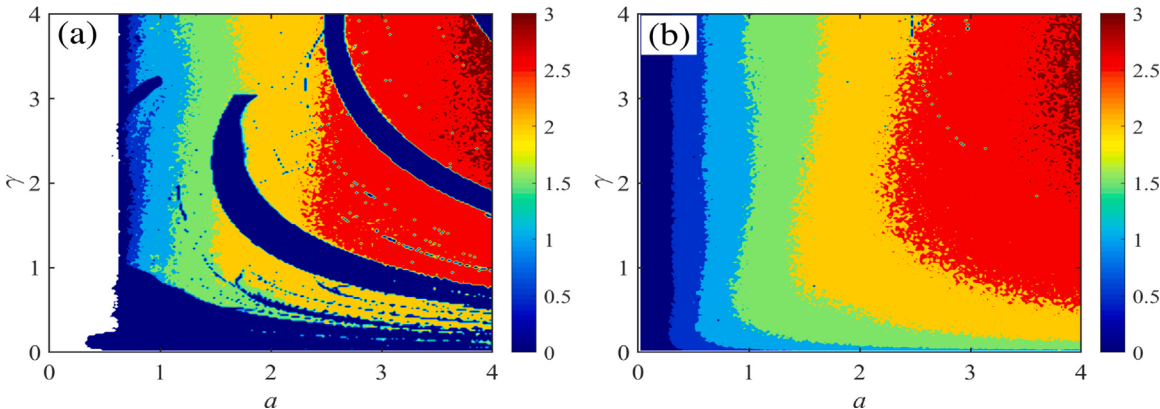


**Fig. 15.** FuzzyEn complexity chaos diagram with  $(a, \omega, \gamma) = (1, \pi, 3)$ . (a) 2D-SIMM. (b) 2D-SIMM-IPM with  $b=1$ .

cases. What is more, it can be seen that SIP<sub>d</sub> with  $\cos(\frac{c}{x})$  has rich dynamics when  $a < 1$ . In addition, the FuzzyEn complexity of IPM<sub>d</sub> with  $c$  variation is presented in Fig. 6. It shows the value of complexity stabilizes at around 3 as  $c$  increases. Thus, we choose the parameter  $c = 100$  when the complexity reaches 3 early for the following study.

### (3) Summary

In conclusion, IPM with single-perturbation affects the attractor phases density. The unbounded perturbation function  $e^x$  focuses on improving the performance of the system when  $a > 1$ , while the bounded perturbation function  $\cos(\frac{c}{x})$  improves the performance of the system at  $a \in [0, 1]$ .

## Case with multiple-perturbations

The previous analysis obtained  $e^x$  and  $\cos(\frac{c}{x})$  which can effectively improve the system performance obviously. In this section, we use

these two perturbations to construct IPM with multiple-perturbations. moreover, we further apply IPM with multiple-perturbations to Sine map and two Sine series maps.

### The enhanced Sine map

Applying IPM with multiple-perturbations to Sine map, the new map (**S-IPM**) is written as

$$x_{n+1} = a \sin[\pi(x_n - b(e^x + \cos(\frac{c}{x})))]. \quad (9)$$

### (1) Equilibrium points and phase diagrams

From the previous analysis, S-IPM exists equilibrium point. Let

$$\begin{cases} y_1 = x \\ y_2 = a \sin(\pi(x - b(e^x + \cos(\frac{c}{x})))) \end{cases}, \quad (10)$$

the equilibrium points are the intersection of  $y_1$  and  $y_2$ . The gray curve and blue curve in Fig. 7 represent  $y_1$  and  $y_2$ , respectively.  $y_2$  exhibits a

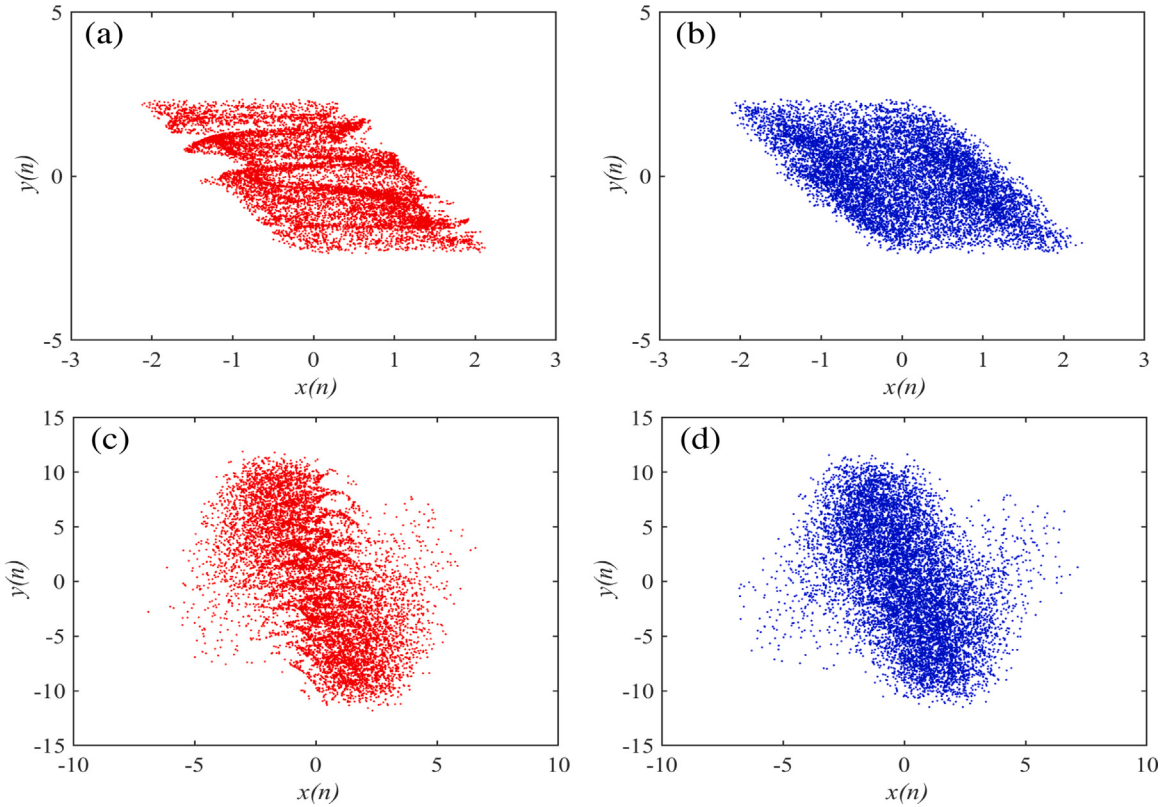


**Fig. 16.** The phase diagrams with  $(x_0, y_0, A, B) = (0.3, 0.3, 1.4, 0.3)$ . (a) FSH with  $v = 0.5$ . (b) FSH-IPM with  $v = 0.5$ . (c) FSH with  $v = 0.1$ . (d) FSH-IPM with  $v = 0.1$ .

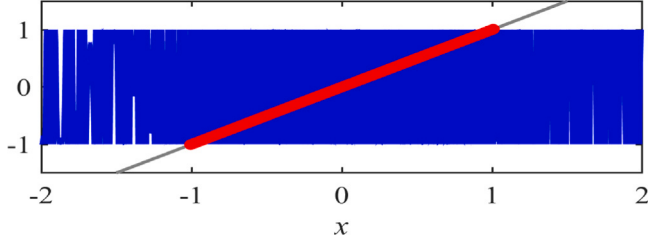


**Fig. 17.** The equilibrium points of FSH-IPM.

certain degree of oscillation curve in the near zero interval. Therefore, for any  $a, b$  within the effective interval, the two curves have infinite many intersections at  $x \in (0_-, 0_+)$ .

The initial value and control parameters are selected as  $x_0=0.1$  and  $(a, b)=(3, 1)$ , respectively. The trajectory of S-IPM in Fig. 8(b) is different from that of Sine map in Fig. 8(a). Compared with the Sine map, the phase diagram of S-IPM presents a planar with better ergodicity and more complex topology.

#### (2) Bifurcation diagram and Lyapunov exponents

The bifurcation diagram and Lyapunov exponents for parameter  $a$  and output  $x_n$  are plotted to analyze the dynamic behavior of chaotic maps further. Let  $x_0 = 0.1$ , step-size 0.02 and  $b=1$ . The bifurcation and Lyapunov exponents of S-IPM map are plotted in Fig. 9. S-IPM has few periodic windows at  $a \in (3.58, 3.60)$  and  $a = (1.1, 1.18)$ . LEs are stable at 5. Compared with Sine map, S-IPM has higher Lyapunov exponents and wider range of chaos.

#### (3) FuzzyEn complexity analysis

Set  $(m, r, N) = (2, 0.15, 1000)$  and  $x_0 = 0.1$ . The FuzzyEn complexity chaos diagram is shown in Fig. 10. It combine the advantages of IPM<sub>b</sub> and IPM<sub>d</sub>, and the maximum complexity is 4.5. Obviously, the performance of the system is improved by perturbations. Furthermore,

discuss the complexity of the system when one parameter is fixed. The blue line represents the complexity value of S-IPM varies  $b$  from 1 to 2 with  $a = 4$  and stabilizes at 3.6. The red line represents the complexity value of S-IPM varies  $a$  from 1 to 4 with  $b = 1$ , which gradually increases.

In addition, a comparison of complexity of S-IPM and other maps is carried out in Fig. 11. Compared with different maps of same dimension and higher dimension, S-IPM always has higher complexity and wider chaos range.

Further, we introduce IPM for two Sine-series maps. The following two factors are considered in determining the position of the perturbation term: (1) The original map contains a unique Sine item, and there is only one state variable in the Sine item. For the above situation, the position of the perturbation item is unique. (2) The original map contains multiple Sine items, or Sine item contain multiple state variables. For these two cases, theoretically, each state variable in each Sine term can be added with a perturbation term, but the final choice of which position is determined by the performance of the new map. We use complexity as a measure. Under the same initial conditions, the average complexity of the new maps within the fixed parameter range is solved, and the position of the perturbation term corresponding to the map with the highest complexity is selected.

#### The enhanced 2D-SIMM map

2D-SIMM map was proposed by Liu et al. [37], which derived from Sine map and ICMIC map. The equation for 2D-SIMM is written as

$$\begin{cases} x_{n+1} = a \sin(\omega y_n) \sin(\gamma/x_n) \\ y_{n+1} = a \sin(\omega x_{n+1}) \sin(\gamma/y_n) \end{cases}, \quad (11)$$

where  $a, \omega, \gamma$  are system parameters, and  $a, \omega, \gamma \in (0, +\infty)$ . Applying IPM with multiple-perturbation to the  $y_n$  of the first dimension of Eq. (11), we can obtain the new map (SIMM-IPM) as follows:

$$\begin{cases} x_{n+1} = a \sin[\omega y_n - b(e^{y_n} + \cos(c/y_n))] \sin(\gamma/x_n) \\ y_{n+1} = a \sin(\omega x_{n+1}) \sin(\gamma/y_n) \end{cases}. \quad (12)$$

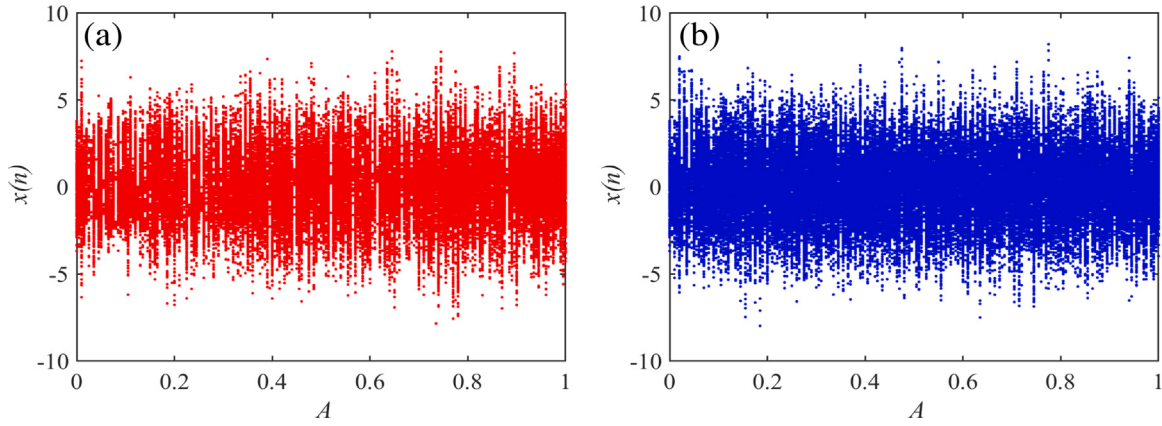


**Fig. 18.** The bifurcation diagrams with  $(x_0, y_0, A, B) = (0.3, 0.3, 1.4, 0.5)$ . (a) FSH with  $v = 0.1$ . (b) FSH-IPM with  $v = 0.1$ .

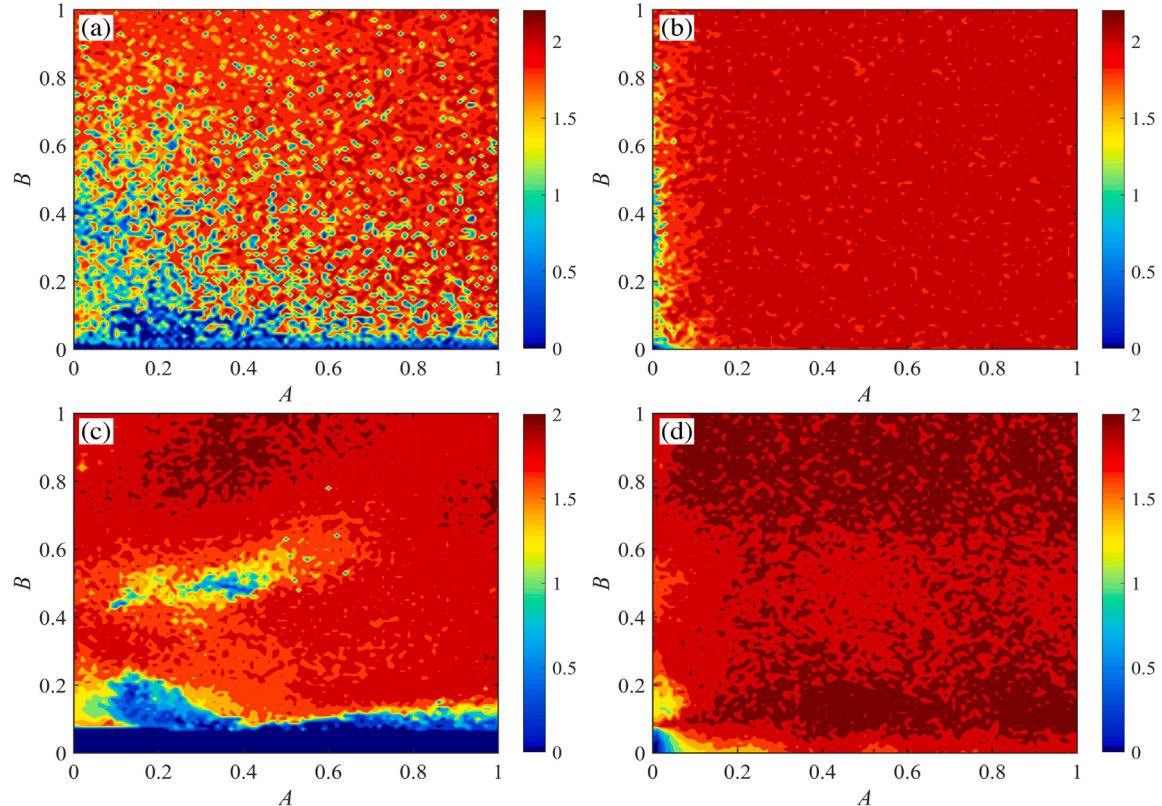


**Fig. 19.** FuzzyEn complexity chaos diagram with  $(x_0, y_0) = (0.3, 0.3)$ . (a) FSH map with  $v = 0.5$ . (b) FSH-IPM map with  $v = 0.5$ . (c) FSH map with  $v = 0.1$ . (d) FSH-IPM map with  $v = 0.1$ .

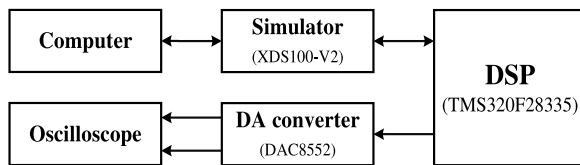


**Fig. 20.** Block diagram of DSP implementation.

### (1) Equilibrium points and phase diagrams

According to the method of Fig. 7, the solution of the equilibrium point is converted into the calculation of the intersection. Similarly, the

equilibrium transformation equation of 2D-SIMM-IPM

$$\begin{cases} y_1 = x \\ y_2 = y \\ y_3 = a \sin(\omega y_2 - b(e^{y_2} + \cos(c/y_2))) \sin(\gamma/y_1) \\ y_4 = a \sin(\omega y_3) \sin(\gamma/y_3) \end{cases} \quad (13)$$

is given and visualized. Fig. 12 shows that the 2D-SIMM-IPM has infinite many equilibrium points.

The initial condition and control parameters are selected as  $(x_0, y_0) = (0.1, 0.1)$  and  $(a, \omega, \gamma) = (1, \pi, 3)$ . As shown in Fig. 13, the attractors of 2D-SIMM and 2D-SIMM-IPM have similar structure. The disappearance of density lines in phase trajectory diagram indicates the increase of the ergodicity and randomness of system with the perturbation controller IPM.

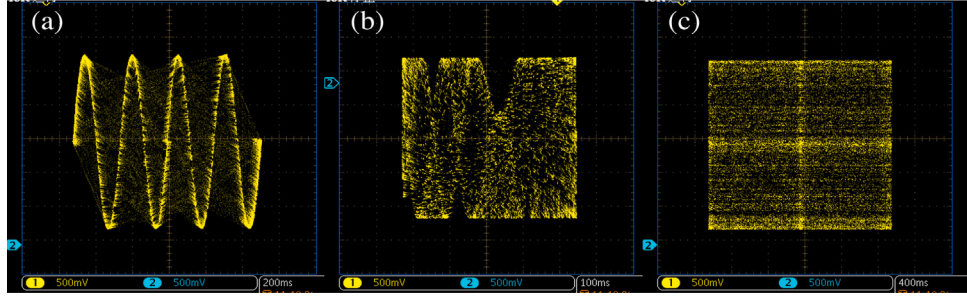


Fig. 21. DSP diagrams of (a) Sine map (b) S-IPM with  $b=0.6$  (c) S-IPM with  $b=1$ .

### (2) Bifurcation diagram and Lyapunov exponents

When  $(\omega, \gamma) = (\pi, 3)$ , the maximum Lyapunov exponents (MLE) versus  $a$  and the corresponding bifurcation diagram are shown in Fig. 14. 2D-SIMM falls into chaos at  $a = 0.82$  and there are several apparent periodic windows at  $a \in (1.66, 1.82) \cup (2.64, 2.88)$  and  $a = (2.18, 2.32)$ . However, 2D-SIMM-IPM has global chaos in the whole parameter range, and its MLE is higher and stable at about 6.5.

### (3) FuzzyEn complexity analysis

Set  $(m, r, N) = (2, 0.15, 2000)$  and  $x_0 = 0.1$ . The FuzzyEn complexity chaos diagram is shown as Fig. 15. The white region in Fig. 15(a) means 2D-SIMM is emanative. The system has large areas of low complexity in the parameter space  $(a - \gamma)$ . For 2D-SIMM-IPM in Fig. 15(b), the low complexity region of the system is greatly reduced and the parameter space is expanded. The complexity values show a relatively orderly increase from left to right.

### The enhanced FSH map

FSH [32] was proposed based on the discrete fractional calculus [38] and sine chaotification model [12] of Hénon map [39]. It is denoted as

$$\begin{cases} x_n = x_0 + \frac{1}{\Gamma(v)} \sum_{j=1}^n \frac{\Gamma(n-j+v)}{\Gamma(n-j+1)} \times (\sin(\pi(y_{j-1} + 1 - Ax_{j-1}^2)) - x_{j-1}) \\ y_n = y_0 + \frac{1}{\Gamma(v)} \sum_{j=1}^n \frac{\Gamma(n-j+v)}{\Gamma(n-j+1)} \times (\sin(\pi Bx_{j-1}) - y_{j-1}) \end{cases}, \quad (14)$$

where  $A$  and  $B$  are control parameters and  $v$  is the order of map. Applying IPM with multiple-perturbation to the  $x_n$  of the first dimension of Eq. (14), the mathematical equation is obtained by

$$\begin{cases} x_n = x_0 + \frac{1}{\Gamma(v)} \sum_{j=1}^n \frac{\Gamma(n-j+v)}{\Gamma(n-j+1)} \times \\ (\sin(\pi(y_{j-1} + 1 - A(x_{j-1} - b(e^{x_{j-1}} + \cos(\frac{c}{x_{j-1}}))^2))) - x_{j-1}) \\ y_n = y_0 + \frac{1}{\Gamma(v)} \sum_{j=1}^n \frac{\Gamma(n-j+v)}{\Gamma(n-j+1)} \times (\sin(\pi Bx_{j-1}) - y_{j-1}) \end{cases}, \quad (15)$$

we call it as FSH-IPM.

### (1) Equilibrium points and phase diagrams

Set  $(x_0, y_0, A, B) = (0.3, 0.3, 1.4, 0.3)$  and discard the first 20000 points. The attractors of FSH and FSH-IPM with  $v = 0.5$  and  $v = 0.1$  are plotted in Fig. 16. The introduce of IPM improves the ergodic property of the system and leads to the distribution of phase points more uniform without change the original topology. Similarly, the solution of the equilibrium point is visualized as an intersection. Fig. 17 shows that the FSH-IPM has infinite many equilibrium points.

### (2) Bifurcation diagram

Ref. [32] demonstrated that FSH has the best dynamic characteristics when  $v = 0.1$  through comparative analysis. Fig. 18 depicts that IPM promotes more than 10 period windows of the original system to the chaotic state. In addition, the FSH-IPM is global chaos.

### (3) FuzzyEn complexity analysis

Furthermore, FuzzyEn based contour plots are applied to visualize the effectiveness of the controller IPM in the parameters regions. For comparison, the complexity performance of FSH and FSH-IPM with  $v = 0.1$  and  $v = 0.5$  are depicted in Fig. 19. The parameters and initial values are the same as before. As the values of the two parameters change, it is obvious that the controller has suppressed the chaos degradations and the FSH-IPM has higher complexity.

### Digital circuit implementation

To further verify the feasibility of the method in digital circuits, we apply the DSP technique to the IPM. Fig. 20 shows the DSP hardware design block diagram. 150MHz floating-point 32-bit chip TMS320F28335 is used to connect the computer with DSP equipment. The generated chaotic sequence is converted into analog signal by digital-to-analog converter DAC8552 and captured on oscilloscope.

As shown in Fig. 21, (a) is the phase diagram of Sine map without perturbation displayed by oscilloscope, (b) and (c) are the phase diagrams of IPM with different perturbation coefficients. As the perturbation coefficient  $b$  changes, the phase point spreads to the entire plane. The experimental results of the digital circuit further prove the effectiveness of the IPM.

### Conclusions

In the endeavor of chaotification, this paper proposed the internal perturbation model with single-perturbation and multiple-perturbations. Perturbation is firstly determined by the single-perturbation, then the better perturbations are selected and superimposed on the original system by multiple-perturbations. We applied IPM to Sine map since it is involved in the construction and modulation of many high-dimensional chaotic systems. Based on the IPM of Sine map, the performance of high-dimensional map with sine items can also be greatly improved. Meanwhile, the topological structure of the system can be remained, and the distribution is more uniform. Therefore, we further promoted IPM to two Sine-series maps (one is an integer-order map and another is a fractional-order map). The dynamics of these maps are analyzed by means of phase diagrams, bifurcation diagrams, Lyapunov exponents and FuzzyEn complexity. Numerical analysis demonstrates that the IPM maps expand the range of chaos and enhance the ergodicity of the original system with fixed parameters. The results of FuzzyEn complexity chaos diagram show that IPM maps have complex dynamic characteristics and higher complexity. The implementation of digital circuit further verifies the feasibility of IPM method in practice. Furthermore, for HD maps, IPM can be introduced to any state variable in any dimension, which reduces chaotification costs. With the IPM, many discrete chaotic systems can be improved. These enhanced chaotic systems will become potential models for secure communication, encryption, pseudorandom sequence generator and other related applications.

## CRediT authorship contribution statement

**Chunyi Dong:** Methodology, Software, Investigation, Writing – original draft, visualization. **Karthikeyan Rajagopal:** Methodology, Formal analysis, Writing – review and editing. **Shaobo He:** Methodology, Validation, Investigation, Writing – original draft, Supervision, Funding acquisition. **Sajad Jafari:** Conceptualization, Writing – review and editing. **Kehui Sun:** Conceptualization, Validation, Formal analysis, Writing – review and editing, Project administration.

## Declaration of competing interest

The authors declare that they have no known competing financial interests or personal relationships that could have appeared to influence the work reported in this paper.

## Acknowledgments

This work was supported by the Natural Science Foundation of China (Nos. 61901530, 62071496, 62061008), the Natural Science Foundation of Hunan Province, China (No. 2020JJ5767), and the Innovation Project of Graduate of Central South University, China (No. 2021zzts0517).

## References

- [1] Lorenz E. Deterministic nonperiodic flow. *J Atmos Sci* 1963;20(2):130–41.
- [2] May R. Simple mathematical models with very complicated dynamic. *Nature* 1976;261:459–67.
- [3] Gong L, Deng C, Pan S. Image compression-encryption algorithms by combining hyper-chaotic system with discrete fractional random transform. *Opt Laser Technol* 2018;103:48–58.
- [4] Li C, Chen G. Chaos in the fractional order chen system and its control. *Chaos Solitons Fractals* 2004;22(3):549–54.
- [5] Lv M, Wang C, Ren G. Model of electrical activity in a neuron under magnetic flow effect. *Nonlinear Dynam* 2016;85(3):1479–90.
- [6] Ma J, Wu F, Wang C. Synchronization behaviors of coupled neurons under electromagnetic radiation. *Internat J Modern Phys B* 2016;31(2):1650251.
- [7] Wang L, Cheng H. Pseudo-random number generator based on logistic chaotic system. *Entropy* 2019;21(10):960.
- [8] Bahramian A, Nouri A, Baghdadi G. Introducing a chaotic map with a wide range of long-term memory as a model of patch-clamped ion channels current time series. *Chaos Solitons Fractals* 2019;126:361–8.
- [9] Khan M, Shah T, Mahmood H. An efficient method for the construction of block cipher with multi-chaotic systems. *Nonlinear Dynam* 2013;71(3):489–92.
- [10] Chen F, Ding Z, Lu Z, Zeng X. Parameters identification for chaotic systems based on a modified jaya algorithm. *Nonlinear Dynam* 2018;94(4):2307–26.
- [11] Lin L, Shen M, et al. Convergence analysis for initial condition estimation in coupled map lattice systems. *IEEE Trans Signal Process* 2012;60(8):4426–32.
- [12] Hua Z, Zhou B, Zhou Y. Sine chaotification model for enhancing chaos and its hardware implementation. *IEEE Trans Ind Electron* 2019;66(2):1273–84.
- [13] Decai L, Min H. Chaotic time series prediction based on a novel robust echo state network. *IEEE Trans Neural Netw Learn Syst* 2012;23(5):787–95.
- [14] Li C, Li S, Asim M. On the security defects of an image encryption scheme. *Image Vis Comput* 2009;27(9):1371–81.
- [15] Natiq H, Banerjee S, Ariffin M. Can hyperchaotic maps with high complexity produce multistability? *Chaos* 2019;29(1):1152–63.
- [16] Li H, Hua Z, Bao H, Zhu L, Chen M, Bao B. Two-dimensional memristive hyperchaotic maps and application in secure communication. *IEEE Trans Ind Electron* 2021;68(10):9931–40.
- [17] Xiao Y, Sun K, He S. Dynamics of a hyperchaotic map with spherical attractor. *Phys Scr* 2020;95(6):065215.
- [18] Xiao Y, Sun K, He S. Constructing chaotic map with multi-cavity. *Eur Phys J Plus* 2020;135(1):21–35.
- [19] Chen G, Mao Y, Chui C. A symmetric image encryption scheme based on 3D chaotic cat maps. *Chaos Solitons Fractals* 2004;21(3):749–61.
- [20] Abdulaziz O, Sun K, Ai W. Design new chaotic maps based on dimension expansion. *Chin Phys B* 2019;28(2):147–55.
- [21] Wang G, Fang Y. Cascade chaos and its dynamic characteristics. *Acta Phys Sin* 2013;62(2):103–12.
- [22] Li C, Sprott J. Variable-boostable chaotic flows. *Optik Int J Light Electron Opt* 2016;127(22):10389–98.
- [23] Wang L, Sun K, Peng Y, He S. Chaos and complexity in a fractional-order higher-dimensional multicavity chaotic map. *Chaos Solitons Fractals* 2020;131:109488.
- [24] Ye X, Wang X. Characteristic analysis of a simple fractional-order chaotic system with infinitely many coexisting attractors and its DSP implementation. *Phys Scr* 2020;95(7):075212.
- [25] Bao H, Hua Z, Li H, Chen M, Bao B. Discrete memristor hyperchaotic maps. *IEEE Trans Circuits Syst I Regul Pap* 2021. <http://dx.doi.org/10.1109/TCSI.2021.3082895>.
- [26] Bao H, Hua Z, Li H, Chen M, Bao B. Memristor-based hyperchaotic maps and application in AC-GANs. *IEEE Trans Ind Inform* 2021. <http://dx.doi.org/10.1109/TII.2021.3119387>.
- [27] Li K, Bao H, Li H, Ma J, Hua Z, Bao B. Memristive Rulkov neuron model with magnetic induction effects. *IEEE Trans Ind Inf* 2021. <http://dx.doi.org/10.1109/TII.2021.3086819>.
- [28] Li J, Liu H. Colour image encryption based on advanced encryption standard algorithm with two-dimensional chaotic map. *IET Inform Secur* 2013;7(4):265–70.
- [29] Hua Z, Zhou Y, Pun C. 2D Sine-logistic modulation map for image encryption. *Inform Sci* 2015;297:80–94.
- [30] Wu Y. Image encryption using the two-dimensional logistic chaotic map. *Electron Imaging* 2012;21(1):013014.
- [31] Yuan F, Deng Y, Li Y. A cascading method for constructing new discrete chaotic systems with better randomness. *Chaos* 2019;29(5):053120.
- [32] Li Y, He X, Zhang W. The fractional difference form of sine chaotification model. *Chaos Solitons Fractals* 2020;137:109774.
- [33] Brown M. Chaos and nonlinear dynamics: an introduction for scientists and engineers. *Shock Vib* 2018;3(3):235.
- [34] Pincus S. Approximate entropy as a measure of system complexity. *Proc Natl Acad* 1991;88:2297–301.
- [35] Chen W, Zhuang J. Measuring complexity using FuzzyEn, ApEn, and SampEn. *Med Eng Phys* 2009;29:61–8.
- [36] Sun K, He S, Yin L. Application of FuzzyEn algorithm to the analysis of complexity of chaotic sequence. *Acta Phys Sin* 2012;61(13):71–7.
- [37] Liu W, Sun K, He S. SF-SIMM high-dimensional hyperchaotic map and its performance analysis. *Nonlinear Dynam* 2017;89:2521–32.
- [38] Chen F, Luo X, Zhou Y. Existence results for nonlinear fractional difference equation. *Southeast Asian Bull Math* 2012;36(1):23–34.
- [39] Hénon M. A two-dimensional mapping with a strange attractor. *Commun Math Phys* 1976;50(1):69–77.